High Sensitivity of Compound Drought and Heatwave Events to Global Warming in the Future

Qin Zhang [1], Liping Zhang [1,2,*], Dunxian She [1,2,*], Gangsheng Wang [1,2], Jie Chen [1,2], and Zengchao Hao [3]

[1] State Key Laboratory of Water Resources and Hydropower Engineering Science, Wuhan University, Wuhan, 430072, China

[2] Institute for Water-Carbon Cycles and Carbon Neutrality, Wuhan University, Wuhan, 430072, China.

[3] College of Water Sciences, Beijing Normal University, Beijing 100875, China

*Corresponding authors: Liping Zhang, zhanglp@whu.edu.cn

Dunxian She, shedunxian@whu.edu.cn

Key points:

- Multi-model ensembles average can capture the historical changes of compound drought and heatwave events well.
- There is a significantly increasing trend for compound drought and heatwave characteristics over almost global land in the future.
- Future will witness higher sensitivity of compound drought and heatwave events to global warming over most global land.

Abstract

Compound drought and heatwave (CDHW) events have received considerable attention in recent years due to their devastating effects on human society and ecosystem. In this study, we systematically investigated the spatiotemporal changes of CDHW events for historical period (1951-2014) and four future scenarios (2020-2100) (SSP1-2.6, SSP2-4.5, SSP3-7.0, and SSP5-8.5) over global land by using Coupled Model Intercomparison Project Phase 6 (CMIP6) models. The sensitivity of the CDHW events to the changes of maximum air temperature and the climatic water balance variables are also examined. The CDHW is defined by integrating monthly standardized precipitation evapotranspiration index (SPEI) and daily maximum temperatures. The results show that the multi-model ensembles project a strong increasing trend in CDHW characteristics over almost all global lands under SSP2-4.5, SSP3-7.0, and SSP5-8.5. A significant increase in CDHW risk will witness across global land areas for the medium to long term future, if there is not aggressive adaptation and mitigation strategies. The results of sensitivity analysis suggest that higher sensitivity of CDHW events to global warming will occur in the future except SSP1-2.6. Particularly, each 1°C global warming increases the duration of the CDHW events by 3 days in the historical period, but by about 10 days in the future period. Overall, this study improves our understanding in the projection of

CDHW events and the impacts of climate drivers to the CDHW events under various future scenarios, which could provide support about the risk assessment, adaptation and mitigation strategies under climate change.

Plain Language Summary

Compound drought and heatwave (CDHW) events (co-occurring hot and dry extremes) always cause severe damages to human society and natural system, often beyond separate impacts from heatwaves and droughts. Understanding the change of CDHW events under global warming can help to manage the risks of associated disasters and advance climate change adaptation. Therefore, we systematically investigated the future changes of CDHW events (characterized by duration, severity, and magnitude) and the relationship between CDHW characteristics and the relevant climate factors using the state-of-the-art climate simulations. Here we show that future will witness a strong increase in CDHW events. A significantly increasing CDHW risk will occur across most global land for the medium to long term future without aggressive adaptation and mitigation strategies. In addition, compared with the historical period, higher sensitivity of CDHW events to global warming over most global land will occur in the future. These tell us that measures to limit the temperature increase are urgently needed for survive and thrive.

Keywords: Compound events, Compound drought and heatwave (CDHW), CMIP6, Sensitivity analysis, Climate change, Future projection

1. Introduction

It is an established fact that the increasing concentration of greenhouse gases caused by human activities has warmed the earth system, including the atmosphere, ocean and land, further accelerating the hydrological cycle (IPCC, 2021; Byrne & O'Gorman, 2018; Tett et al., 1999; P. Wu et al., 2013). The increase in global surface temperature alters the spatiotemporal pattern, frequency and magnitude of extreme events, such as heatwave (Perkins-Kirkpatrick & Lewis, 2020; Russo et al., 2014), drought (Ault, 2020; Dai, 2011; Trenberth et al., 2014; G. Wu et al., 2022), heavy precipitation (Fischer & Knutti, 2016; Min et al., 2011; Morrison et al., 2019) and flood (Gudmundsson et al., 2021; Hirabayashi et al., 2013). Considerable attention has been paid to the research in weather and climate extremes in recent decades due to the severe social and economic impacts (Alexander et al., 2006; Cook et al., 2020; Wang et al., 2021; Q. Zhang et al., 2021). Given the dependence between relevant climate drivers or hazards, some extreme events tend to occur concurrently, such as drought and heatwave, heavy rain and strong wind, which are termed compound events (Field et al., 2012; Zscheischler et al., 2018; Zscheischler & Seneviratne, 2017). Compared with single extreme events, compound events generally have much more devastating effects on natural and human systems, especially for compound drought and heatwave (CDHW) events, as its large spatial extent and long duration (Mukherjee & Mishra, 2021; Shi et al., 2021; Zscheischler et al., 2018; Zscheischler & Seneviratne, 2017). Hence, it is essential to investigate the spatiotem-

poral variation of the CDHW events, especially their climate driving factors during historical and future periods for risk assessment, adaptation and mitigation strategies.

Recently, many studies have investigated the characteristics of CDHW events in various temporal and spatial scales and found that the frequency of CDHW events has increased over the observed period and will continue to increase under high future emission scenarios in most regions across the globe (Mukherjee & Mishra, 2021; X. Wu et al., 2020; P. Zhang et al., 2020; Zscheischler & Seneviratne, 2017). In addition, various methods were proposed to quantify and describe the characteristics and risks of CDHW events. Some studies (Bevacqua et al., 2021; Leonard et al., 2014; Zscheischler et al., 2018) clarified and extended the concept of compound events, and established the framework of compound event research for quantifying its impacts and risks based on the earlier definitions in the IPCC Special Report on Climate Extremes (IPCC-SREX). Subsequently, some researchers used the percentile of monthly precipitation and temperature (low precipitation percentile and high temperature percentile) to describe the variation of dry-hot climate condition (X. Wu et al., 2020; Zhou & Liu, 2018; Zscheischler & Seneviratne, 2017). In the past few years, an increasing number of studies investigated the variation of CDHW characteristics by defining CDHW event as a heatwave episode that occurs under drought conditions (Feng et al., 2020; Mukherjee et al., 2020; Mukherjee & Mishra, 2021). In these studies, the Standardized Precipitation Index (SPI) or Palmer Drought Severity Index (PDSI) were employed to identify drought events, while a heatwave was typically defined as a period of consecutive extremely hot days with the daily maximum temperature (Tmax) above a fixed percentile (Feng et al., 2020; Mukherjee & Mishra, 2021; Shi et al., 2021; Yu & Zhai, 2020).

Generally, previous attention mainly focuses on the description of CDHW event characteristics (Feng et al., 2020; Hao et al., 2018; X. Wu et al., 2019), and the changes of CDHW events during the historical period using observations (Feng et al., 2020; Mukherjee & Mishra, 2021; Yu & Zhai, 2020) and climate model simulations (Nina N. Ridder et al., 2021). For the projection of future period, several studies focused on the projection changes of CDHW by using the percentile of monthly precipitation and temperature to describe the dry-hot climate conditions, and only limited future scenario was selected, such as, the Representative Concentration Pathway (RCP) 8.5 scenario from Coupled Model Intercomparison Project Phase 5 (CMIP5) (X. Wu et al., 2020; Zhou & Liu, 2018; Zscheischler & Seneviratne, 2017). Recently, a state-of-the-art generation of global climate models (GCMs) participating in CMIP6 have been available, which have higher spatial resolution and improvements in physical processes, and these GCMs employ the new Shared Socioeconomic Pathway (SSP)/RCP-based emission scenarios for the future simulations of climate change (Eyring et al., 2016; O'Neill et al., 2016). The results in Nina N. Ridder et al. (2021) show that some CMIP6 models are able to capture the historical characteristics of CDHW events in most regions of the world. Therefore, it is workable to adopt the GCMs from CMIP6 for investigating the variation of CDHW events

over history and the future. Using the CMIP6 multi-model ensemble, Vogel et al. (2020) projected the changes in clusters of extreme dry-hot events at four different global warming levels; Y. Wu et al. (2021) investigated the future changes of compound extremes of monthly temperature and precipitation. So far, however, there has been limited assessments of the projected changes of global CDHW events from the event-based perspective under various future scenarios based on CMIP6 simulations. Additionally, deeper understanding of how relevant climate drivers contribute to the changes of CDHW events characteristics is still lacking. In this study, we systematically explore the spatial-temporal changes of CDHW events over global land areas excluding Antarctica in history (1951-2014) and various future (2020-2100) scenarios (i.e., SSP-RCP scenario), integrating monthly standardized precipitation evapotranspiration index (SPEI) and daily maximum temperatures from CMIP6 models. Furthermore, we examine the sensitivity of CDHW events to the relevant climate influencing factors including Tmax and climatic water deficit (the difference between precipitation and potential evapotranspiration) for a better understanding of the relationship between climate factors and CDHW events under global warming conditions. The specific objectives of this study are to: (1) evaluate the performance of the selected models in simulating the observed CDHW events; (2) investigate the projected changes of global CDHW; and (3) reveal the sensitivity of the changes of CDHW events to climatic driving factors and the relevant contribution rate of climatic driving factors.

2. Materials and Methods

2.1 Data

The six GCMs from CMIP6 are selected for the studies (Table 1). In order to calculate the SPEI for further identifying CDHW events, we downloaded 11 meteorological variables at the daily resolution for the historical simulation period 1950-2014 and the projection period 2015-2100 from the GCMs (Table S1) (Eyring et al., 2016). To consider a range of possible future projection, four combined scenarios of SSPs and RCPs from Tier 1 of ScenarioMIP, are considered, i.e., SSP1-2.6 (+2.6 W/ m^2; low forcing sustainability pathway), SSP2-4.5 (+4.5 W m^2; medium forcing middle of the road pathway), SSP3-7.0 (+7.0 W m^2; high forcing regional rivalry pathway), and SSP5-8.5 (+8.5 W m^2; high forcing fossil-fueled development pathway) (Cook et al., 2020; O'Neill et al., 2016).

Table 1. Information of used GCMs in this study

NUM	Model	Spatial Resolution	Experiments
1	CMCC-CM2-SR5	192×288	Historical SSP2-4.5 SSP3-7.0 SSP5-8.5
2	FGOALS-g3	80×180	Historical SSP1-2.6 SSP2-4.5 SSP3-7.0
3	KACE-1-0-G	144×192	Historical SSP1-2.6 SSP2-4.5 SSP3-7.0 SSP5-8.5
4	NorESM2-LM	96×144	Historical SSP1-2.6 SSP2-4.5 SSP3-7.0 SSP5-8.5
5	NorESM2-MM	192×288	Historical SSP1-2.6 SSP2-4.5 SSP3-7.0 SSP5-8.5

NUM	Model	Spatial Resolution	Experiments
6	UKESM1-0-LL	144×192	Historical SSP1-2.6 SSP2-4.5 SSP3-7.0 SSP5-8.5

In order to validate the ability of GCMs to simulate various climate variables and compound events, some observed records need to be employed. In this study, the global land daily gridded maximum temperature product provided by Climate Prediction Center (CPC-Unified) for the period 1979 to 2014 with a spatial resolution of $0.5^{o}\times0.5^{o}$ is used (PSL. 2022). This dataset has been widely used as a reference for hydro-meteorology studies and climate change impact studies due to the strict quality control and accuracy (Tarek et al. 2021; Mukherjee and Mishra 2021; Nashwan et al. 2019). The monthly precipitation and evapotranspiration baseline data are taken from the Climatic Research Unit gridded Time Series Version 4 (CRU TS4.05) dataset with a 0.5^{o} grid from 1950 to 2014 (Harris et al., 2020). Due to the long time span and high data quality, CRU TS dataset has been widely employed in diverse research areas and applications, especially for climate and hydrological fields (Arnell & Gosling, 2016; Guo et al., 2019; Hao et al., 2018).

Basically, the simulated climate variables from GCMs always have some biases compared to the observed data (Chen et al., 2021). To minimize the biases and improve the accuracy of climate model outputs, we employ the widely-used Quantile Mapping (QM) method (Cannon et al., 2015; Maraun, 2013) to correct the monthly precipitation and Tmax from GCMs outputs, and correct the potential evapotranspiration (PET) calculated by the Penman–Monteith (PM) equation using the 11 meteorological variables in table S1. The QM bias correction method is one of the statistical downscaling methods, which attempts to find a transfer function to obtain the best fit in mapping the simulated cumulative distribution function of the variable onto the observed cumulative distribution function (Themeßl et al., 2012). A detailed description of the QM method is provided in A.1. of the Supporting information.

2.2 Definition of compound drought and heatwave events

In our study, the drought is defined in meteorological terms, as a water deficit (difference between precipitation and PET) over a weekly, month or multi-month scale (Vicente-Serrano, et al. 2010). The standardized precipitation evapotranspiration index (SPEI) is applied to identify drought events. Here we calculate SPEI at a 3-month scale (SPEI-3), and the drought event is defined as SPEI-3 $<$ -1 (Li et al., 2020; K. Xu et al., 2015) (Figure 1a). Compared to the other two widely used drought indices, i.e., self-calibrated Palmer drought severity index (sc-PDSI) (Wells et al. 2004) and standardized precipitation index (SPI) (McKee et al. 1995), the SPEI is more suitable for detecting, monitoring and investigating drought characteristics under global warming, as it considers the consequences of PET (which includes solar radiation, temperature, wind speed, air pressure and relative humidity) to drought (Vicente-Serrano et al. 2010). The 3-month time scale SPEI and the fixed threshold value of -1 are

suitable for identifying drought conditions, which have been widely employed to identify drought events over global and regional areas (Hao et al., 2018; Li et al., 2020; Spinoni et al., 2019; K. Xu et al., 2015). We use the Food and Agricultural Organization Penman–Monteith method (FAO-PM) to calculate the PET. The detailed descriptions about FAO-PM method and calculating SPEI are displayed in supplemental materials (Appendix A.2-3).

For the identification of heatwave events, the daily maximum temperature (Tmax) data is used. A heatwave event is defined as Tmax greater than the 95th percentile of the baseline period and lasting at least three days (Figure 1b), which has been widely employed to identify heatwave events in the existing literature (Kong et al., 2020; Z. Xu et al., 2016).

Based on the definition of drought and heatwave events, a CDHW event is referred to as a heatwave event occurring within the drought month in our study (Mukherjee et al., 2020; Mukherjee & Mishra, 2021; Zscheischler et al., 2018). As can be seen from Figure 1, magenta lines are threshold; light yellow shading denotes drought event; the part of Tmax time series marked in red are heatwave events; the heatwave events circled by the orange oval are CDHW events because they occur in drought months.

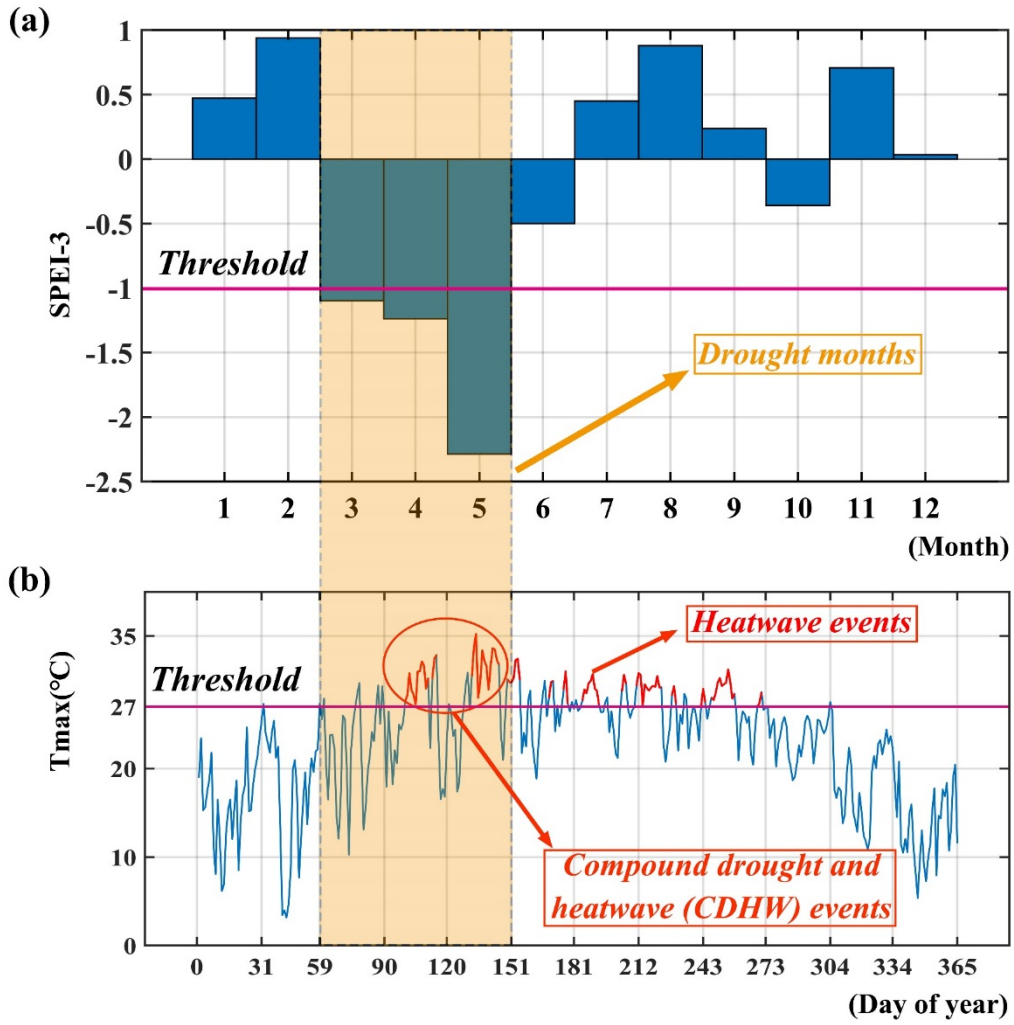

Figure 1. Schematic diagram of the identification of compound drought and heatwave (CDHW) events. Magenta lines are threshold. Light yellow shading denotes drought event. The part of Tmax time series marked in red are heatwave events.

We further characterize the CDHW events using the duration, severity, and magnitude. The characteristics of selected CDHW events are described as follows.

(i) CDHW duration is defined as the total number days of heatwave events during the drought month (SPEI <-1 in this study) per year

(ii) CDHW severity indicates the difference between the average Tmax of CDHW

events and the temperature threshold (95th percentile of a baseline period)

(iii) CDHW magnitude can be described by combining drought conditions and heatwave conditions, which is defined as:

$$M = \frac{1}{N}\sum_{n=1}^{N}\left(T\max_{i} - thre\right) * |\mathrm{SPEI}_i|$$

where M is the magnitude of CDHW events, N is the total days of CDHW events in a year, $T\max_i$ is the Tmax of the n day of CDHW events in a year, $thre$ is the temperature threshold, SPEI_i is the value of SPEI-3 during the month of the n day of CDHW events.

The temporal trend of CDHW characteristics is estimated using the Sen's slope estimator (Sen, 1968), and the Mann-Kendall (MK) trend test (Kendall, 1975; Mann, 1945), which have been widely used in the trend detection of hydrometeorological variables (Feng et al., 2020; Mukherjee & Mishra, 2021). The kernel density estimator, which is a nonparametric method for estimating the empirical probability distribution function (Russo et al., 2014), is employed to explore the variability of future CDHW events relative to the historical period. A detailed description of these methods is given in the supplementary materials (Appendix A.4-5).

2.3 Sensitivity analysis

For investigating how the variation of CDHW events can be attributed to variations of its input factors, we further explore the sensitivity of CDHW events to the temperature and the water deficit index (WDI, i.e., difference between precipitation and PET). The linear regression analysis method is adopted in this study, which is the simplest and most widely used sensitivity analysis method (Pianosi et al., 2016).

Here we assume a multiple linear relationship $y = a_i + b_i x_i$ exists between the dependent variable (CDHW characteristic) and the explanatory variables (Tmax and WDI). The linear least-squares estimate method is employed to estimate the regression coefficient b_i, which is the sensitivity measure. Given the input factors have different units of measurement, we use the standard regression coefficient to measure the sensitivity, which is defined as follow (Hall et al., 2009; Pianosi et al., 2016):

$$S_i = b_i \frac{\mathrm{SD}(x_i)}{SD(y)}$$

where S_i is the sensitivity coefficient for the input factor i, SD is the standard deviation. In this study, two input factors, i.e., daily maximum temperature (Tmax) and water deficit index (WDI), are selected, and the sensitivity can be characterized as $S_{T\max}$ and S_{WDI}, respectively.

Furthermore, we quantified the contribution of selected factors to the variation of CDHW events. The relative contribution rate can be defined as follow (Tomas-Burguera et al., 2020):

$$\mathrm{CR}_i = \frac{|S_i|}{\sum_{i=1}^{n} |S_i|} \times 100\%$$

where CR_i is the relative contribution rate for the input factor i. The $\mathrm{CR}_{T\,\mathrm{max}}$ and $\mathrm{CR}_{\mathrm{WDI}}$ stand for the contribution rate of Tmax and WDI, respectively.

3. Results

3.1 Performance of GCM simulations

To examine the capacity of the multi-model ensemble in reproducing the climate drivers for identifying CDHW events, we firstly assess the performance of the raw and corrected multi-model ensembles average in simulating the Tmax (Figure 1.), precipitation (Figure S1) and PET (Figure S2). For the spatial distributions, we randomly select a year of the historical period (1998 in this study) as an example rather than a multi-year average. The results show that both raw and corrected multi-model ensembles mean can well capture the spatial patterns, of which the latter matches the observed data better for all three variables. The correlation coefficients of the corrected variables are all greater than the raw data, whose values are greater than 0.975. For the temporal change over global land areas, we find that the raw multi-model ensembles tend to underestimate the annual average of Tmax, and overestimate the precipitation and PET, while the corrected one fits the observed data well for both variations and trends. Compared with the Tmax and PET, the precipitation of raw and corrected data perform poorly in representing fluctuations (Figure S1d).

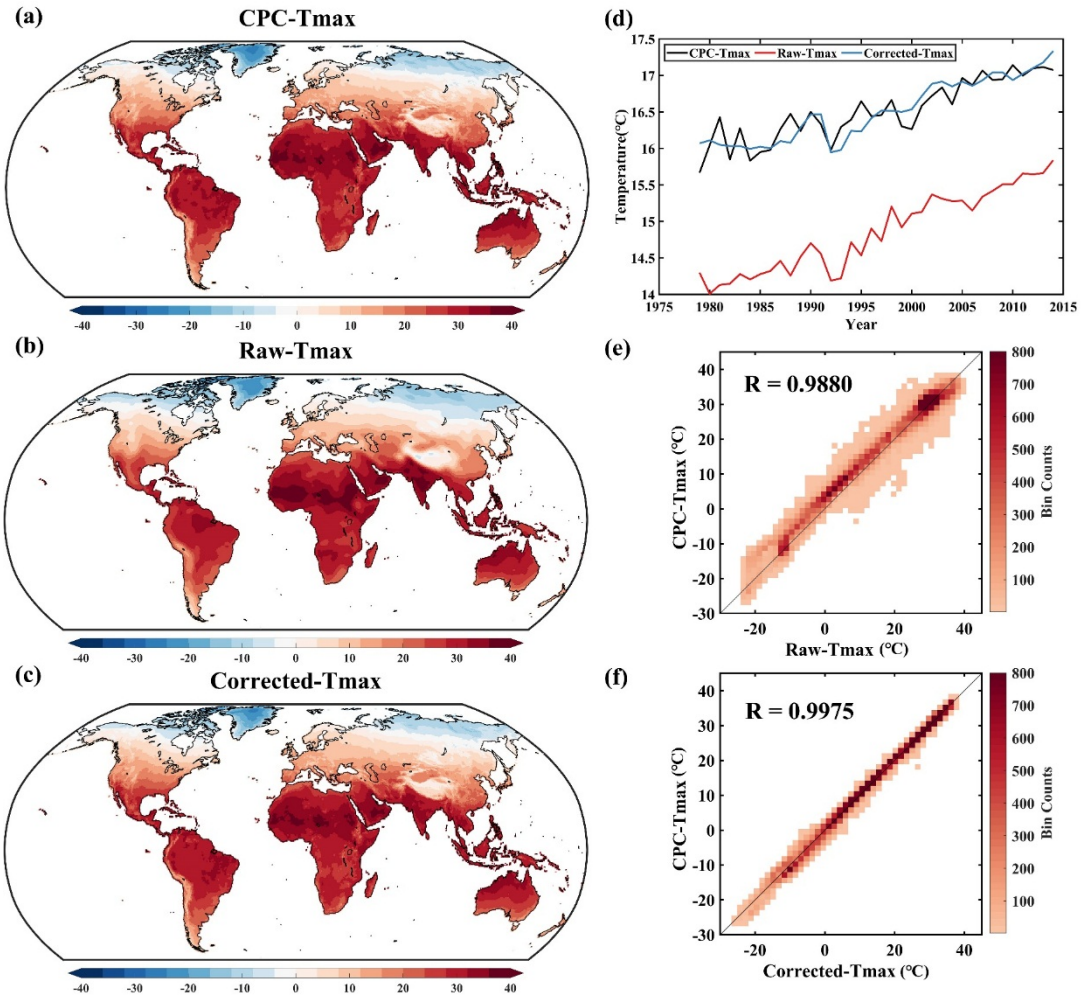

Figure 2. Bias correction performance of annual average daily maximum temperature (Tmax) from multi-model ensemble for 1979-2014 over global land areas. (a) Spatial distribution of observed Tmax from CPC-unified in 1998; (b) Spatial distribution of raw multi-model ensemble mean Tmax in 1998; (c) Spatial distribution of corrected multi-model ensemble mean Tmax in 1998; (d) Change in global land Tmax for 1979-2014; (e) Bin scatter of the raw Tmax and CPC Tmax for all global land pixels in 1998;(f) Bin scatter of the corrected Tmax and CPC Tmax for all global land pixels in 1998.

We also compare the CDHW characteristics of historical corrected simulation with that of observed data during 1979-2014 from the spatial distributions and temporal changes, including CDHW magnitude (Figure 3), duration (Figure S3), and severity (Figure S4). As can be seen from these figures, the spatial patterns of simulated CDHW characteristics are largely consistent with the observations;

however, there are some local discrepancies between simulated and observed data, such as the Amazon basin and parts of North East Asia for CDHW magnitude. The results for bin-scatters further confirm the consistency of spatial distributions between the observed CDHW characteristics and the simulated CDHW characteristics. The correlation coefficients for the CDHW characteristics in magnitude and severity are larger than 0.78. For the temporal change of CDHW characteristics (Figure 3c, Figure S3c, and Figure S4c), we find that the simulated CDHW characteristics capture the trend of time series well for the historical period. Meanwhile, a significant increasing trend for all three CDHW characteristics can be detected during the historical period (1979-2014), and the increasing trend is more pronounced especially from 1995 (0.0493/decade for 1979-1995 and 0.2678/decade for 1996-2014 in CDHW magnitude).

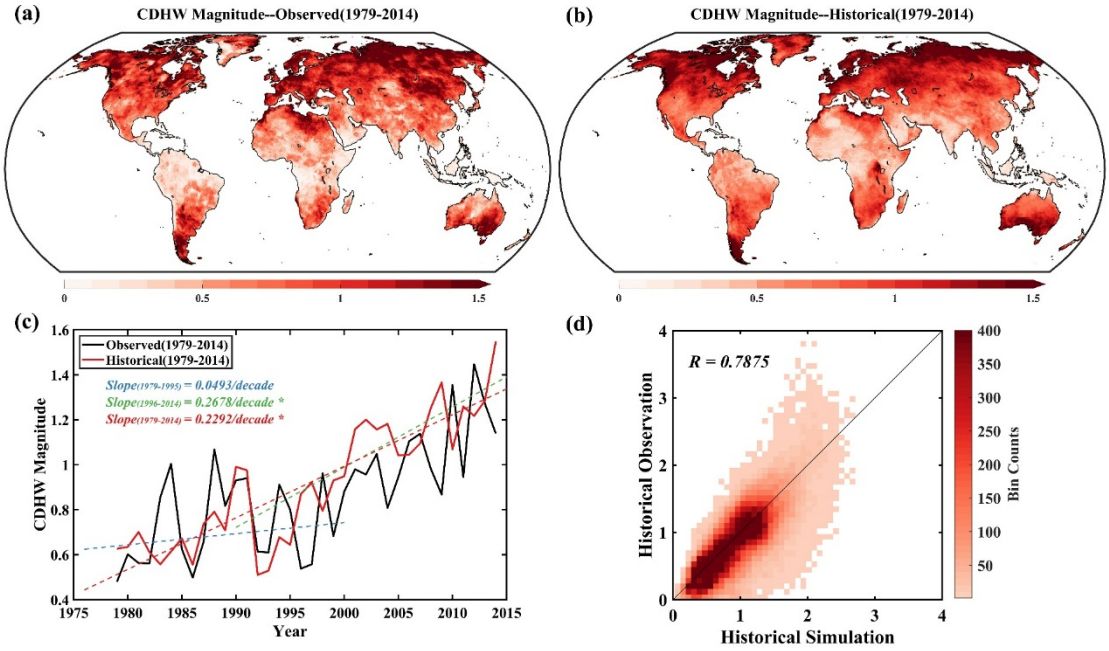

Figure 3. Comparisons of spatiotemporal patterns of CDHW magnitude for 1979-2014 from observed data and corrected multi-model ensemble mean, respectively. (a) The observed mean spatial patterns of CDHW magnitude; (b) The historical simulated mean spatial patterns of CDHW magnitude; (c) Time series of CDHW magnitude for 1979-2014, the solid black line represents the historical observation, and the solid red line represents the historical simulation. The dashed lines represent linear fits, and the symbol "*" denotes a significant trend at a 0.05 significance level. (d) The bin-scatter between the historical observation and simulation for all global land pixels.

Taken together, the corrected multi-model ensemble average from CMIP6 models can capture the spatial patterns and temporal changes of annual Tmax, precipitation, PET, and diverse CDHW characteristics well. Especially, the

changes in the trend of climate drivers and diverse CDHW characteristics from the multi-model ensemble mean are quite consistent with that of observed data in the historical period. Hence, we inferred that it is rational to project the CDHW characteristics using CMIP6 models for different scenarios over the future period, which will be presented in the subsequent subsection.

3.2 Projection changes of CDHW characteristics

The global average changes and variabilities for diverse CDHW characteristics are displayed in Figure 4 for historical and future periods. For future projection, all four scenarios show a significantly increasing trend. The CDHW characteristics trajectories across the four future scenarios diverge most strongly after 2050. The time series of CDHW characteristics tends to stabilize after 2050 under SSP1-2.6 due to the low emissions and more aggressive mitigations. While the global average CDHW characteristics will continue to increase under other scenarios, of which the SSP5-8.5 scenario has the fastest riser, followed by SSP3-7.0 and SSP2-4.5. The historical simulations reproduce the observed means and variances from the kernel density charts, which agree with the results of Figure 3. Meanwhile, there are larger means and variances under SSP2-4.5, SSP3-7.0, and SSP5-8.5 scenarios, while the SSP1-2.6 has a similar variance and the larger mean compared with the historical period.

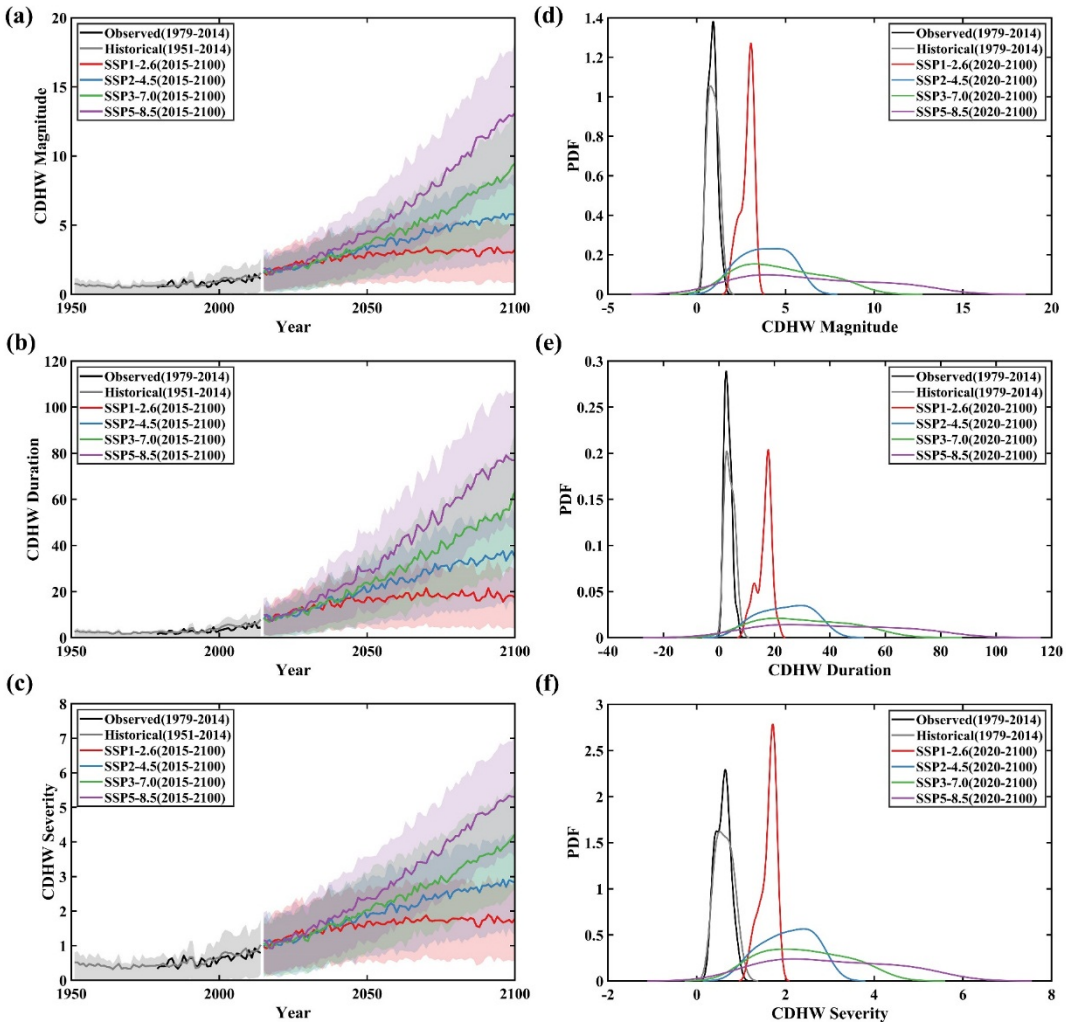

Figure 4. Time series and probability density function (PDF) of global annual average CDHW characteristics including magnitude (a, d), duration (b, e), and severity (c, f) for the historical simulation (grey lines), observed (black lines) and future projections from four scenarios. The shaded areas denote the interquartile range calculated across models.

Furthermore, we explore the spatial distributions of trends for CDHW magnitude (Figure 5), CDHW duration (Figure S5), and CDHW severity (Figure S6). Generally, the spatial distributions of the trend changes are largely consistent for different CDHW characteristics. As Figure 5 shows, there is a significantly increasing trend of CDHW magnitude in almost all land surface regions globally under SSP2-4.5, SSP3-7.0, and SSP5-8.5, while half of the global land areas has no significant trend for the historical simulation and SSP1-2.6. Notably for

SSP5-8.5, the CDHW events are characterized by greater than 1 ℃ per decade increase in CDHW magnitude, greater than 10 days per decade increase in CDHW duration and greater than 0.5℃ per decade increase in CDHW severity during the future period (2020-2100) over most regions of the world, including Amazon basin, Circum-Mediterranean regions, Middle East, Western and Northern Asia, Europe, Northern Mexico, most parts of Africa, etc. What is interesting about this figure is Eastern China and India will likely witness a smaller increasing trend, and this region coincides well with the East and South Asian monsoon regions.

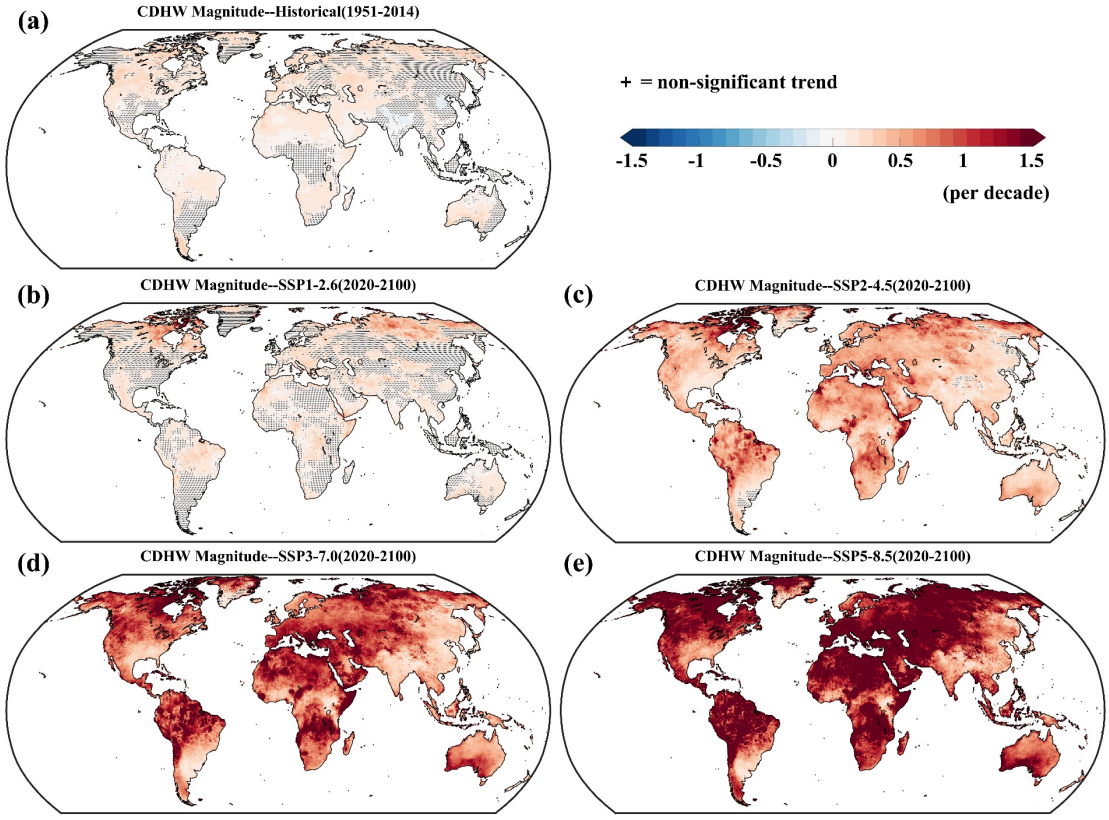

Figure 5. Spatial change patterns of CDHW magnitude for history and four future scenarios. The symbol "+" denotes a non-significant trend at a 0.05 significance level.

We divide the future into three sub time periods, i.e., near term (2021-2040), mid-term (2041-2060), and long term (2081-2100) according to IPCC AR6 to clarify the changes of CDHW during different time periods (IPCC, 2021). The spatial changes maps of CDHW mean characteristics for these three periods under four scenarios relative to the historical reference period (1981-2010) are presented in Figure 6 and Figure S7-S8.

Figure 6 shows that the CDHW magnitude for all three future terms is greater than that of the baseline period over global land areas. In the near term (2021-2040), there is no significant difference in the spatial patterns of CDHW magnitude between the four future scenarios, which is in agreement with the changes of time series in Figure 4a-c. In the long term (2081-2100), more than half of the global land areas including central and northern North America, the Amazon basin, Europe, much of Africa, western and northern Asia, southern Australia, have a CDHW magnitude above 5 under high and very high greenhouse gas emission scenarios (SSP3-7.0 and SSP5-8.5). The smallest CDHW magnitude occurs in the low greenhouse gas emission scenario SSP1-2.6. Additionally, we find that the different CDHW characteristics are largely consistent in spatial distribution. These results suggest that the global land areas will subject to an increasing risk of CDHW events in the medium to long term future without the more aggressive adaptation and mitigation strategies.

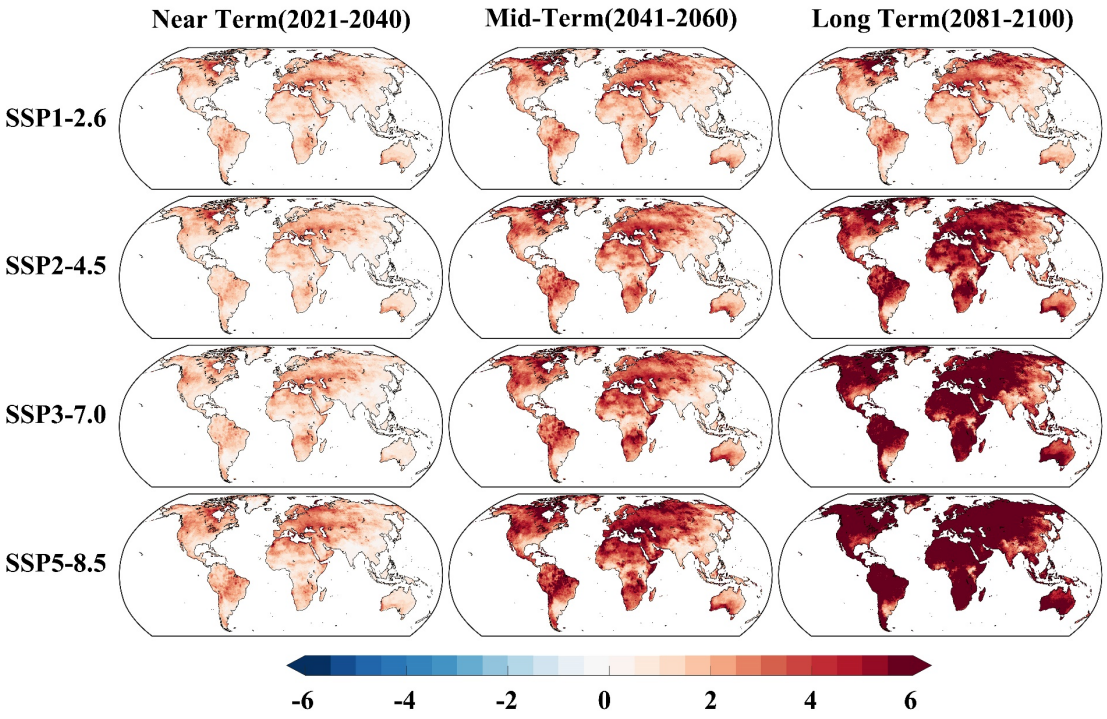

Figure 6. Spatial features of CDHW mean magnitude using 1981-2010 baseline for diverse future scenarios at near term (2021-2040), mid-term (2061-2080) and long term (2081-2100), respectively.

Overall, CMIP6 multi-model ensembles project a strong increasing trend in various CDHW characteristics under all four scenarios. Compared to the historical period, there are larger means and variances under the selected future scenarios except SSP1-2.6. For the spatial changes of CDHW characteristics, there is a

significantly increasing trend in almost all global land areas under SSP2-4.5, SSP3-7.0, and SSP5-8.5. The medium to long-term future will witness an increasing CDHW risk across global land areas in high and very high greenhouse gas emission scenarios (SSP3-7.0 and SSP5-8.5).

3.3 Sensitivity analysis of CDHW events

To investigate the responses of CDHW characteristics to the related climate drivers (Tmax and WDI), we further explore the relative contribution rate of climatic driving variables to the changes of CDHW events using the sensitivity analysis method mentioned in subsection 2.3. In this subsection, we mainly focus on the sensitivity of CDHW magnitude considering the consistency of different CDHW characteristics in temporal and spatial changes.

The sensitivity coefficient boxplots of CDHW magnitude to Tmax and WDI for global land pixels are shown in Figure 7a. In general, high temperature promotes CDHW event, while rich water inhibits it. Therefore, for most of the global land pixels, the $S_{T\max}$ value is positive and the S_{WDI} value is negative. To compare in the boxplot, the absolute value of sensitivity coefficients is calculated. What stands out in this figure is that higher sensitivity of CDHW magnitude to Tmax will occur in the future (except SSP1-2.6) compared to the historical period. This is especially true for the scenario SSP5-8.5, the median of sensitivity coefficients from global land pixels is 0.76 while it is 0.38 in the historical period.

The boxplots of the contribution rate of Tmax and WDI to the CDHW magnitude changes during historical and future period (Figure 7b) indicates that Tmax dominates the CDHW event changes under historical time period, SSP2-4.5, SSP3-7.0, and SSP5-8.5. In addition, a higher contribution rate will occur in future scenarios except SSP1-2.6. The median of contribution rates from global land pixels is 0.75 under SSP5-8.5 while it is 0.53 under the historical period.

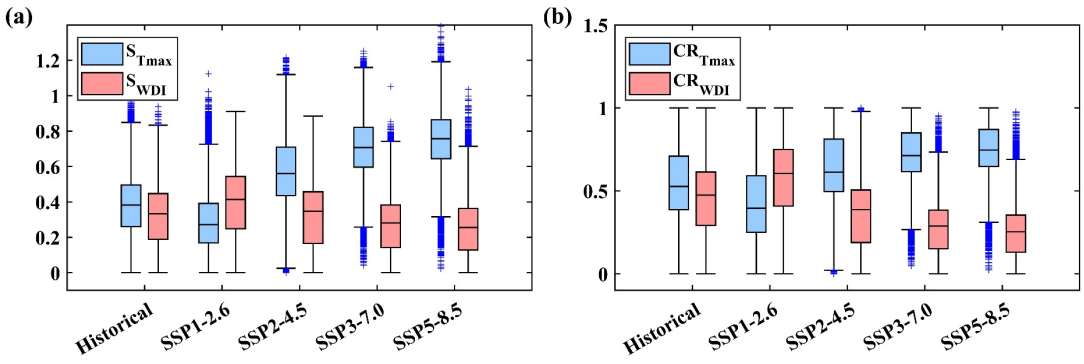

Figure 7. Boxplot of sensitivity analysis of CDHW magnitude (a) and contribution rate of climate drivers to CDHW magnitude (b) for global land pixels under historical simulation and four future scenarios. The $S_{T\max}$ and S_{WDI} de-

note the sensitivity of CDHW magnitude to the annual average daily maximum temperature (Tmax) and annual total water deficit index (WDI), respectively. The $\mathrm{CR}_{T\,\mathrm{max}}$ and $\mathrm{CR}_{\mathrm{WDI}}$ denote the contribution rate of the annual average Tmax and annual WDI to the changes of CDHW magnitude, respectively.

The spatial maps of S_{Tmax} and S_{WDI} for CDHW magnitude are provided in Figure 8. Compared to the historical S_{Tmax}, the future S_{Tmax} significantly increases across most regions of global land except SSP1-2.6. Notably for SSP3-7.0 and SSP5-8.5, more than half of the global land pixels have S_{Tmax} values being greater than 0.7. These pixels are mainly located in the Amazon Basin, western South America, most of Africa, west-central Australia, and the Middle East. For the spatial distributions of S_{WDI}, there are no significant changes between historical and future periods under scenarios SSP2-4.5, SSP3-7.0 and SSP5-8.5. Most of the northern hemisphere corresponds to a much darker blue color, especially for the northern part of Eurasia and northern North America. Overall, the sensitivity coefficients of scenario SSP1-2.6 present different spatial distributions compared with other future scenarios.

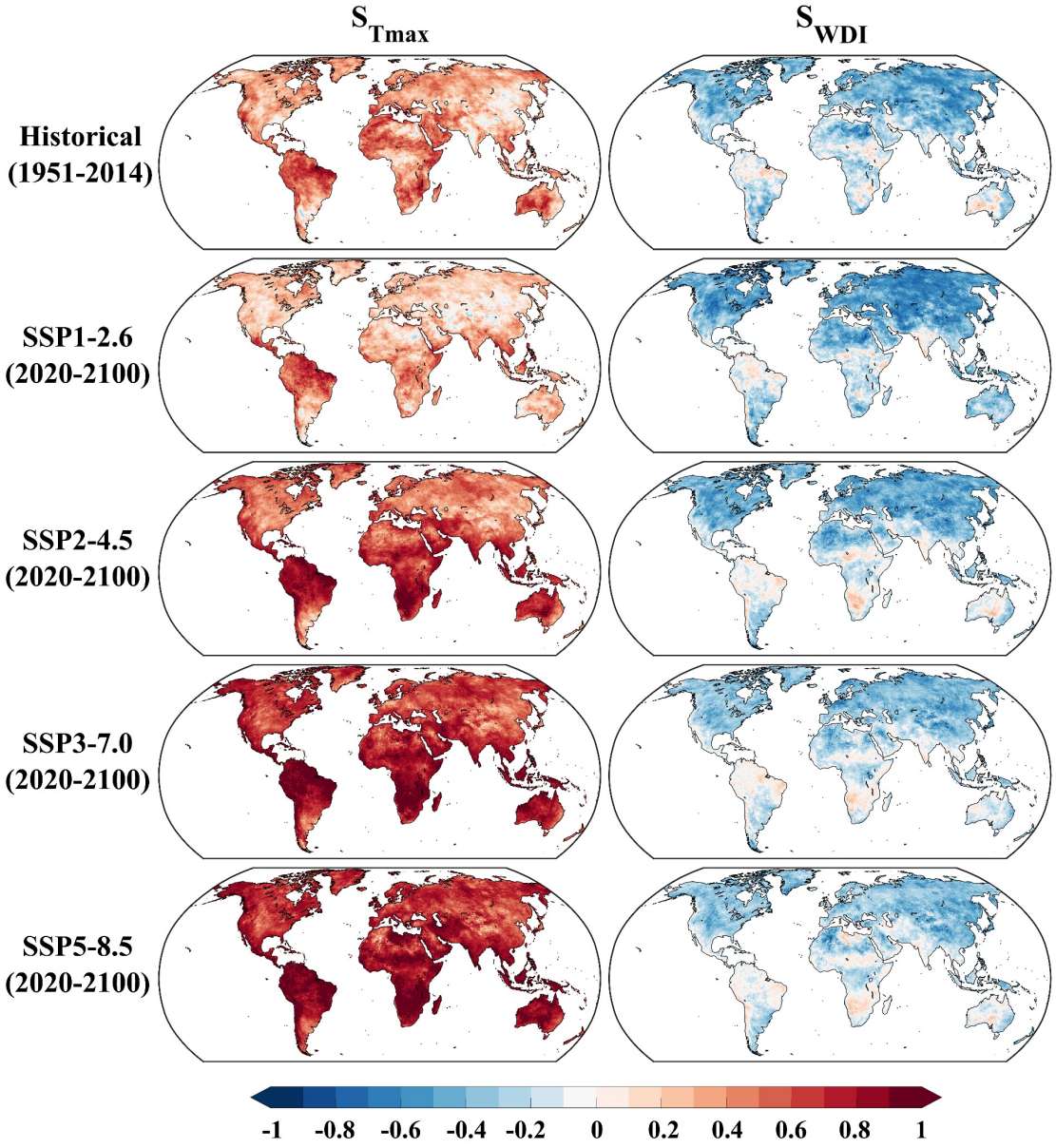

Figure 8. Spatial distributions of sensitivity coefficients including $S_{T\,\max}$ and S_{WDI} for CDHW magnitude under historical period, SSP1-2.6, SSP2-4.5, SSP3-7.0, SSP5-8.5, respectively.

We further present the spatial maps of contribution rate for CDHW magnitude during the historical and future period in Figure 9. According to the definition of $\mathrm{CR}_{T\,\max}$ and $\mathrm{CR}_{\mathrm{WDI}}$, the sum of these two coefficients is 1 for the one fixed

pixel; Hence, we only present one graph for one scenario here. The red color indicates that the temperature change dominates the change of CDHW events, while the blue color indicates that the water deficit change dominates it. The darker the color indicates a higher contribution.

Figure 9 presents the spatial distributions of contribution rate (CR) of climate drivers, of which a pixel with red represents that the Tmax dominates the variation of CDHW magnitude; a pixel with blue represents that the WDI dominates it. As can be seen from this figure, the Tmax change dominates the variation of CDHW magnitude over more than 90% pixels of global land under scenarios SSP3-7.0 and SSP5-8.5. In historical and SSP2-4.5, more than half of the global land pixels still have higher $\mathrm{CR}_{T\,\mathrm{max}}$ value. But for SSP1-2.6, the water deficit dominates the change of CDHW magnitude over 65% global land pixels. Collectively, most blue regions occur over Northern Hemisphere, for example, China, northern Asia, most of North America during the historical period. The scenario SSP1-2.6 will witness an almost blue Northern Hemisphere, while the red regions only occur over India, southeast Asia, central and southern Africa, Amazon Basin. Most of the blue regions in the historical period will turn red in the future except SSP1-2.6. Especially for SSP3-7.0 and SSP5-8.5, temperature changes almost dominated the changes of CDHW characteristics across all global land areas.

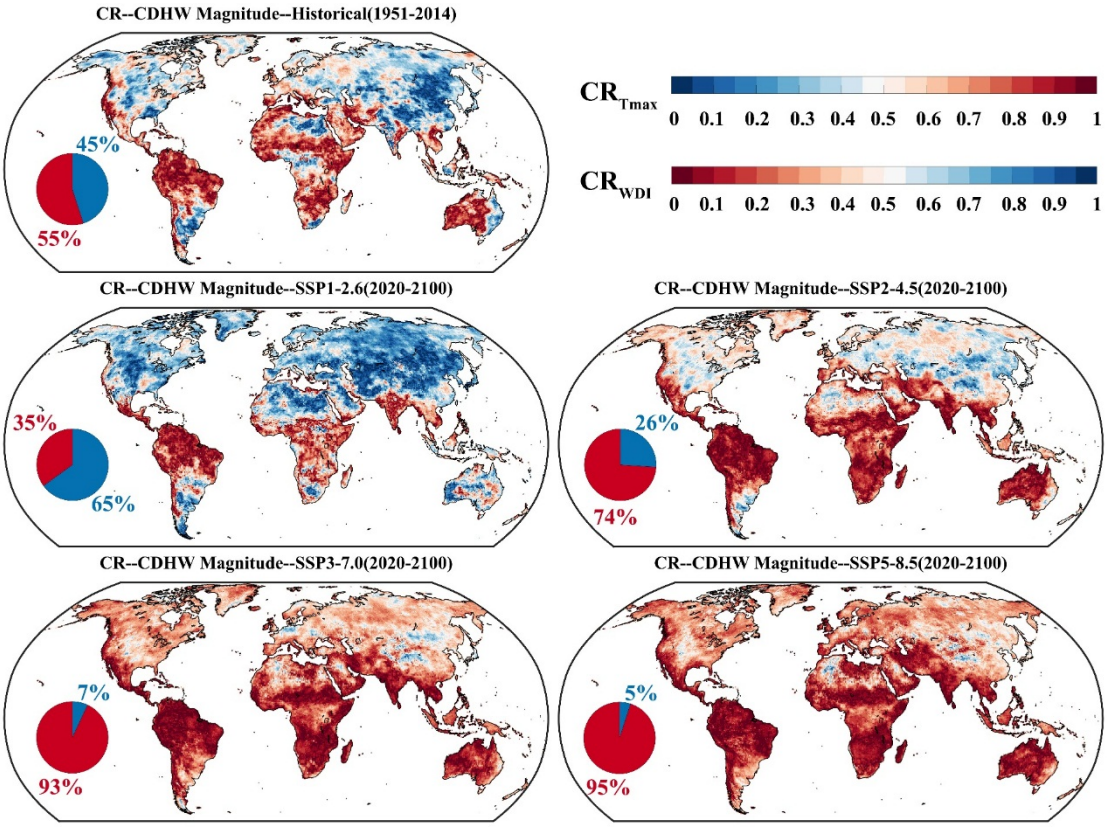

Figure 9. Spatial distributions of contribution rate (CR) including $CR_{T\max}$ and CR_{WDI} for CDHW magnitude under historical period, SSP1-2.6, SSP2-4.5, SSP3-7.0, SSP5-8.5, respectively. Pie-charts represent the percentage of area where temperature (red) and water deficit (blue) dominate the change in CDHW magnitude.

We also find that higher sensitivity of CDHW characteristics to temperature and the higher contribution rate of the changes in temperature to the changes of CDHW characteristics will occur in the future except SSP1-2.6 from these results mentioned above, which suggests a strong relationship between CDHW characteristics and Tmax. Hence, we further explore it from an average global perspective. The changes in global average CDHW magnitude and Tmax are provided in Figure 10a. The trends of CDHW magnitude time series are very consistent with that of Tmax for both historical simulation and future scenarios. Figure 10b present the scatter plot of CDHW magnitude and Tmax. There is a strong relationship between CDHW magnitude and Tmax for both historical and future periods. What is more interesting is that the slope of the future period is significantly larger than that of the historical period, which agrees with the above results and suggests higher sensitivity of CDHW events to global warming in the future.

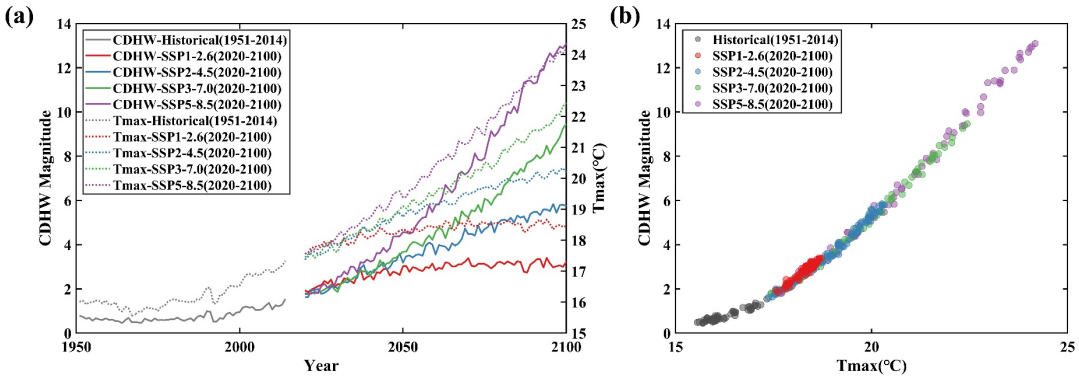

Figure 10. Relationship between CDHW magnitude with global annual average Tmax under historical simulation and four future scenarios. (a) Changes in global average CDHW magnitude and Tmax. Solid lines denote the CDHW magnitude, and dotted lines denote Tmax. (b) Scatter plot of CDHW magnitude and Tmax.

Furthermore, we calculate the slopes of different CDHW characteristics (CDHW duration, severity, and magnitude) to Tmax using the linear regression method under historical simulation and four future scenarios (Table 2). The results show that each 1°C global warming increases the duration of the CDHW event by 3 days in the historical period, but by about 10 days in the future period under four scenarios. In addition, the sensitivity of CDHW magnitude to global warming in the future period is approximately three times greater than that in the historical period.

Table 2. Regression coefficients of different CDHW characteristics to Tmax during historical and future periods.

Scenarios	Historical	SSP1-2.6	SSP2-4.5	SSP3-7.0	SSP5-8.5
Duration (days)	3.12	9.79	10.14	10.77	10.93
Severity (℃)	0.36	0.63	0.64	0.64	0.65
Magnitude	0.55	1.36	1.46	1.57	1.74

4. Discussion

Here, we systematically investigate the projection of CDHW events (characterized by duration, severity, and magnitude) using the state-of-the-art CMIP6 models under four future scenarios. The sensitivity of CDHW events to climate drivers (including Tmax and WDI) is also quantified. We find a strong increasing trend in CDHW characteristics and higher sensitivity of CDHW events to global warming over most global land areas in the future except SSP1-2.6. Nevertheless, there are some points that need to be discussed.

For the historical period, there is a significant temporal increase in the average

CDHW characteristics, notably in recent two decades (Figure 3), which agrees with the previous research about the changes of CDHW based on observed data (Hao et al., 2018; Mukherjee & Mishra, 2021). The overall spatial characteristics of simulated CDHW are in keeping with prior studies, but there are some local discrepancies between our study and previous studies, which might be due to the differences of data, identification method of CDHW event or study period (Feng et al., 2020; Hao et al., 2018; Mukherjee & Mishra, 2021; X. Wu et al., 2019).

We conclude that CDHW events are projected to increase over global land areas, which is in agreement with the existing projection research (N. N. Ridder et al., 2022; Sarhadi et al., 2018; X. Wu et al., 2020; Zscheischler & Seneviratne, 2017). For all future scenarios, it is worth pointing out that Eastern China and India will likely witness a smaller increasing trend in CDHW events (Figure 5-6), and these regions coincide well with the East and South Asian monsoon regions. A possible explanation for this might be that warming is relatively small (Fan et al., 2020), while precipitation significantly increase over these monsoon regions (Z. Chen et al., 2020).

This study find that CDHW events have a high sensitivity to global warming in the future period except SSP1-2.6. There is a possible explanation for this result. In our work, we assume that Tmax and WDI are independent when performing sensitivity analysis. In fact, they are dependent. In general, the increase in temperatures promotes both precipitation and PET (Berg et al., 2013; Kingston et al., 2009; Singleton & Toumi, 2013). With global warming, the dependence between Tmax and precipitation will become stronger, further strengthening the correction between Tmax and WDI in the future period, which will exacerbate the increase in CDHW events (Sarhadi et al., 2018; Zscheischler & Seneviratne, 2017). In short, an increase in temperature has a greater effect on the change of CDHW events in the future period than that in the historical period, i.e., higher sensitivity of CDHW events to global warming in the future.

Recently, an interesting finding that precipitation trends determine future occurrences of compound hot–dry events, was published (Bevacqua et al., 2022). The authors concluded, from the perspective of uncertainty, future droughts will always coincide with at least moderately hot extremes due to the large local warming; however, precipitation trends commonly depend on the model, region and internal climate variability. That is, the uncertainty in the compound dry-hot event arises mainly from the uncertainty in precipitation trends. In a word, future compound hot–dry events are constraint by the constraining regional precipitation trends, which is non-contradictory with our conclusion. We explored the relative contribution of climate drivers to the variation of CDHW events without consideration of uncertainty. Although the multi-model ensembles can simulate the CDHW characteristics well in time series and spatial distribution during the historical period, the model uncertainty (shaded areas in Figure 4) is considerable in the historical period, and even larger in the future period under all scenario. Uncertainty is an inevitable issue in conducting future projection

research. In addition to the model uncertainty mentioned above, the uncertainty can also be derived from observed data, bias correction methods, and future scenarios in our study. The uncertainty should be quantified in further researches.

5. Conclusions

In this study, we investigated the spatiotemporal changes of CDHW characteristic (including CDHW duration, severity, and magnitude) based on the definition of CDHW, using SPEI-3 and Tmax from CMIP6 models under historical period (1951-2014) and diverse future scenarios (2020-2100) including SSP1-2.6, SSP2-4.5, SSP3-7.0, and SSP5-8.5. Furthermore, we explored the responses of CDHW characteristics to related climate drivers (Tmax and WDI) using the sensitivity analysis method. The main conclusions are drawn as follows.

(1) The corrected multi-model ensemble average from CMIP6 simulations can capture the spatial patterns and temporal changes of annual Tmax, precipitation, PET, and diverse CDHW characteristics well. Especially, the changes in the trend of climate drivers and diverse CDHW characteristics from the multi-model ensemble mean are quite consistent with that of observed data in the historical period.

(2) For the future period, CMIP6 multi-model ensembles project a strong increasing trend in various global average CDHW characteristics under all four scenarios, and there is a significantly increasing trend in CDHW characteristics over almost all global land under SSP2-4.5, SSP3-7.0, and SSP5-8.5. The medium to long term future will witness an increasing CDHW risk across global land under scenarios SSP3-7.0 and SSP5-8.5.

(3) There is a higher sensitivity of CDHW events to global warming in the future period (2020-2100) compared with that in the historical period (1951-2014). The changes in Tmax dominate the changes of CDHW events over most global land areas under future scenarios except SSP1-2.6. Particularly, each 1°C global warming increases the duration of the CDHW event by 3 days in the historical period, but by about 10 days in the future period.

This study improves the understanding in the projected changes of CDHW events and the impacts of climate drivers to the CDHW event under various future scenarios, which could provide useful information for the risk management of compound events and implementation of adaptation and mitigation strategies under climate change.

Acknowledgment

This study was supported by the National Key Research and Development Program of China (No.2017YFA0603704), National Natural Science Foundation of China (No.41877159), Major projects of the National Natural Science Foundation of China (No.41890824), and the Strategic Priority Research Program of the Chinese Academy of Sciences (No. XDA23040500).

Data Availability Statement

CMIP6 models data is available at https://esgf-node.llnl.gov/projects/cmip6/. The global land daily gridded maximum temperature product provided by Climate Prediction Center (https://psl.noaa.gov/data/gridded/data.cpc.globaltemp.html). The monthly precipitation and evapotranspiration baseline data are taken from the Climatic Research Unit gridded Time Series Version 4 (CRU TS4.05) dataset (https://www.uea.ac.uk/groups-and-centres/climatic-research-unit).

References

https://psl.noaa.gov/data/gridded/data.cpc.globaltemp.html

Alexander, L. V., Zhang, X., Peterson, T. C., Caesar, J., Gleason, B., Klein Tank, A. M. G., et al. (2006). Global observed changes in daily climate extremes of temperature and precipitation. *Journal of Geophysical Research Atmospheres*, *111*(5), 1–22. https://doi.org/10.1029/2005JD006290Arnell, N. W., & Gosling, S. N. (2016). The impacts of climate change on river flood risk at the global scale. *Climatic Change*, *134*(3), 387–401. https://doi.org/10.1007/s10584-014-1084-5Ault, T. R. (2020). On the essentials of drought in a changing climate. *Science*, *368*(6489), 256–260. https://doi.org/10.1126/SCIENCE.ABC4034Berg, P., Moseley, C., & Haerter, J. O. (2013). Strong increase in convective precipitation in response to higher temperatures. *Nature Geoscience*, *6*(3), 181–185. https://doi.org/10.1038/ngeo1731Bevacqua, E., De Michele, C., Manning, C., Couasnon, A., Ribeiro, A. F. S., Ramos, A. M., et al. (2021). Guidelines for Studying Diverse Types of Compound Weather and Climate Events. *Earth's Future*, *9*(11). https://doi.org/10.1029/2021EF002340Bevacqua, E., Zappa, G., Lehner, F., & Zscheischler, J. (2022). Precipitation trends determine future occurrences of compound hot–dry events. *Nature Climate Change*. https://doi.org/10.1038/s41558-022-01309-5Byrne, M. P., & O'Gorman, P. A. (2018). Trends in continental temperature and humidity directly linked to ocean warming. *Proceedings of the National Academy of Sciences of the United States of America*, *115*(19), 4863–4868. https://doi.org/10.1073/pnas.1722312115Cannon, A. J., Sobie, S. R., & Murdock, T. Q. (2015). Bias correction of GCM precipitation by quantile mapping: How well do methods preserve changes in quantiles and extremes? *Journal of Climate*, *28*(17), 6938–6959. https://doi.org/10.1175/JCLI-D-14-00754.1Chen, J., Arsenault, R., Brissette, F. P., & Zhang, S. (2021). Climate Change Impact Studies: Should We Bias Correct Climate Model Outputs or Post-Process Impact Model Outputs? *Water Resources Research*, *57*(5), 1–22. https://doi.org/10.1029/2020WR028638Chen, Z., Zhou, T., Zhang, L., Chen, X., Zhang, W., & Jiang, J. (2020). Global Land Monsoon Precipitation Changes in CMIP6 Projections. *Geophysical Research Letters*, *47*(14). https://doi.org/10.1029/2019GL086902Cook, B. I., Mankin, J. S., Marvel, K., Williams, A. P., Smerdon, J. E., & Anchukaitis, K. J. (2020). Twenty-First Century Drought Projections in the CMIP6 Forcing Scenarios. *Earth's Future*, *8*(6). https://doi.org/10.1029/2019EF001461Dai, A. (2011). Drought under

global warming: A review. *Wiley Interdisciplinary Reviews: Climate Change*, *2*(1), 45–65. https://doi.org/10.1002/wcc.81Eyring, V., Bony, S., Meehl, G. A., Senior, C. A., Stevens, B., Stouffer, R. J., & Taylor, K. E. (2016). Overview of the Coupled Model Intercomparison Project Phase 6 (CMIP6) experimental design and organization. *Geoscientific Model Development*, *9*(5), 1937–1958. https://doi.org/10.5194/gmd-9-1937-2016Fan, X., Duan, Q., Shen, C., Wu, Y., & Xing, C. (2020). Global surface air temperatures in CMIP6: Historical performance and future changes. *Environmental Research Letters*, *15*(10). https://doi.org/10.1088/1748-9326/abb051Feng, S., Wu, X., Hao, Z., Hao, Y., Zhang, X., & Hao, F. (2020). A database for characteristics and variations of global compound dry and hot events. *Weather and Climate Extremes*, *30*, 100299. https://doi.org/10.1016/j.wace.2020.100299Field, C. B., Barros, V., Stocker, T. F., & Dahe, Q. (Eds.). (2012). *Managing the Risks of Extreme Events and Disasters to Advance Climate Change Adaptation*. *Managing the Risks of Extreme Events and Disasters to Advance Climate Change Adaptation*. Cambridge: Cambridge University Press. https://doi.org/10.1017/CBO9781139177245Fischer, E. M., & Knutti, R. (2016). Observed heavy precipitation increase confirms theory and early models. *Nature Climate Change*, *6*(11), 986–991. https://doi.org/10.1038/nclimate3110Gudmundsson, L., Boulange, J., Do, H. X., Gosling, S. N., Grillakis, M. G., Koutroulis, A. G., et al. (2021). Globally observed trends in mean and extreme river flow attributed to climate change. *Science*, *371*(6534), 1159–1162. https://doi.org/10.1126/science.aba3996Guo, Q., Chen, J., Zhang, X., Shen, M., Chen, H., & Guo, S. (2019). A new two-stage multivariate quantile mapping method for bias correcting climate model outputs. *Climate Dynamics*, *53*(5–6), 3603–3623. https://doi.org/10.1007/s00382-019-04729-wHall, J. W., Boyce, S. A., Wang, Y., Dawson, R. J., Tarantola, S., & Saltelli, A. (2009). Sensitivity Analysis for Hydraulic Models. *Journal of Hydraulic Engineering*, *135*(11), 959–969. https://doi.org/10.1061/(asce)hy.1943-7900.0000098Hao, Z., Hao, F., Singh, V. P., & Zhang, X. (2018). Changes in the severity of compound drought and hot extremes over global land areas. *Environmental Research Letters*, *13*(12). https://doi.org/10.1088/1748-9326/aaee96Harris, I., Osborn, T. J., Jones, P., & Lister, D. (2020). Version 4 of the CRU TS monthly high-resolution gridded multivariate climate dataset. *Scientific Data*, *7*(1), 109. https://doi.org/10.1038/s41597-020-0453-3Hirabayashi, Y., Mahendran, R., Koirala, S., Konoshima, L., Yamazaki, D., Watanabe, S., et al. (2013). Global flood risk under climate change. *Nature Climate Change*, *3*(9), 816–821. https://doi.org/10.1038/nclimate1911IPCC, 2021: Summary for Policymakers. In: Climate Change 2021: The Physical Science Basis. Contribution of Working Group I to the Sixth Assessment Report of the Intergovernmental Panel on Climate Change [Masson-Delmotte, V., P. Zhai, A. Pirani, S. L. Connors, C. Péan, S. Berger, N. Caud, Y. Chen, L.Goldfarb, M. I. Gomis, M. Huang, K. Leitzell, E. Lonnoy, J.B.R. Matthews, T. K. Maycock, T. Waterfield, O. Yelekçi, R. Yu and B. Zhou (eds.)]. Cambridge University Press. In Press.Kendall, M. G. (1975). *Rank Correlation Methods (4th edn.) Charles Griffin. San Francisco, CA*.Kingston, D. G., Todd, M. C., Taylor, R.

G., Thompson, J. R., & Arnell, N. W. (2009). Uncertainty in the estimation of potential evapotranspiration under climate change. *Geophysical Research Letters*, *36*(20). https://doi.org/10.1029/2009GL040267Kong, Q., Guerreiro, S. B., Blenkinsop, S., Li, X. F., & Fowler, H. J. (2020). Increases in summertime concurrent drought and heatwave in Eastern China. *Weather and Climate Extremes*, *28*, 100242. https://doi.org/10.1016/j.wace.2019.100242Leonard, M., Westra, S., Phatak, A., Lambert, M., van den Hurk, B., Mcinnes, K., et al. (2014). A compound event framework for understanding extreme impacts. *Wiley Interdisciplinary Reviews: Climate Change*, *5*(1), 113–128. https://doi.org/10.1002/wcc.252Li, L., She, D., Zheng, H., Lin, P., & Yang, Z.-L. (2020). Elucidating Diverse Drought Characteristics from Two Meteorological Drought Indices (SPI and SPEI) in China. *Journal of Hydrometeorology*, *21*(7), 1513–1530. https://doi.org/10.1175/JHM-D-19-0290.1Mann, H. B. (1945). Mann Nonparametric test against trend. *Econometrica*, (13), 245–259.Maraun, D. (2013). Bias correction, quantile mapping, and downscaling: Revisiting the inflation issue. *Journal of Climate*, *26*(6), 2137–2143. https://doi.org/10.1175/JCLI-D-12-00821.1McKee T.B., Doesken N.J., K. J. (1995). Drought monitoring with multiple time scales. *Proceedings of the 9th Conference on Applied Climatology*, 233–236. Retrieved from http://www.americanbanker.com/issues/179_124/which-city-is-the-next-big-fintech-hub-new-york-stakes-its-claim-1068345-1.html%5Cnhttp://www.ncbi.nlm.nih.gov/pubmed/15003161%
S. K., Zhang, X., Zwiers, F. W., & Hegerl, G. C. (2011). Human contribution to more-intense precipitation extremes. *Nature*, *470*(7334), 378–381. https://doi.org/10.1038/nature09763Morrison, A., Villarini, G., Zhang, W., & Scoccimarro, E. (2019). Projected changes in extreme precipitation at sub-daily and daily time scales. *Global and Planetary Change*, *182*(July), 103004. https://doi.org/10.1016/j.gloplacha.2019.103004Mukherjee, S., & Mishra, A. K. (2021). Increase in Compound Drought and Heatwaves in a Warming World. *Geophysical Research Letters*, *48*(1). https://doi.org/10.1029/2020GL090617Mukherjee, S., Ashfaq, M., & Mishra, A. K. (2020). Compound Drought and Heatwaves at a Global Scale: The Role of Natural Climate Variability-Associated Synoptic Patterns and Land-Surface Energy Budget Anomalies. *Journal of Geophysical Research: Atmospheres*, *125*(11), 0–19. https://doi.org/10.1029/2019JD031943Nashwan, M. S., Shahid, S., & Chung, E.-S. (2019). Development of high-resolution daily gridded temperature datasets for the central north region of Egypt. *Scientific Data*, *6*(1), 138. https://doi.org/10.1038/s41597-019-0144-0NOAA Physical Sciences Laboratory (PSL). 2022. [accessed April 5, 2022]O'Neill, B. C., Tebaldi, C., van Vuuren, D. P., Eyring, V., Friedlingstein, P., Hurtt, G., et al. (2016). The Scenario Model Intercomparison Project (ScenarioMIP) for CMIP6. *Geoscientific Model Development*, *9*(9), 3461–3482. https://doi.org/10.5194/gmd-9-3461-2016Perkins-Kirkpatrick, S. E., & Lewis, S. C. (2020). Increasing trends in regional heatwaves. *Nature Communications*, *11*(1), 1–8. https://doi.org/10.1038/s41467-020-16970-7Pianosi, F., Beven, K., Freer, J., Hall, J. W., Rougier, J., Stephenson, D. B., & Wagener, T. (2016). Sensitivity analysis of environmental models: A systematic review

with practical workflow. *Environmental Modelling and Software*, *79*, 214–232. https://doi.org/10.1016/j.envsoft.2016.02.008Riahi, K., van Vuuren, D. P., Kriegler, E., Edmonds, J., O'Neill, B. C., Fujimori, S., et al. (2017). The Shared Socioeconomic Pathways and their energy, land use, and greenhouse gas emissions implications: An overview. *Global Environmental Change*, *42*(1), 153–168. https://doi.org/10.1016/j.gloenvcha.2016.05.009Ridder, N. N., Pitman, A. J., & Ukkola, A. M. (2021). Do CMIP6 Climate Models Simulate Global or Regional Compound Events Skillfully? *Geophysical Research Letters*, *48*(2), 1–11. https://doi.org/10.1029/2020GL091152Ridder, N. N., Ukkola, A. M., Pitman, A. J., & Perkins-Kirkpatrick, S. E. (2022). Increased occurrence of high impact compound events under climate change. *Npj Climate and Atmospheric Science*, *5*(1), 3. https://doi.org/10.1038/s41612-021-00224-4Russo, S., Dosio, A., Graversen, R. G., Sillmann, J., Carrao, H., Dunbar, M. B., et al. (2014). Magnitude of extreme heat waves in present climate and their projection in a warming world. *Journal of Geophysical Research Atmospheres*, *119*(22), 12,500-12,512. https://doi.org/10.1002/2014JD022098Sarhadi, A., Ausín, M. C., Wiper, M. P., Touma, D., & Diffenbaugh, N. S. (2018). Multidimensional risk in a nonstationary climate: Joint probability of increasingly severe warm and dry conditions. *Science Advances*, *4*(11). https://doi.org/10.1126/sciadv.aau3487Sen, P. K. (1968). Estimates of the Regression Coefficient Based on Kendall's Tau. *Journal of the American Statistical Association*, *63*(324), 1379–1389. https://doi.org/10.1080/01621459.1968.10480934Shi, Z., Jia, G., Zhou, Y., Xu, X., & Jiang, Y. (2021). Amplified intensity and duration of heatwaves by concurrent droughts in China. *Atmospheric Research*, *261*(April), 105743. https://doi.org/10.1016/j.atmosres.2021.105743Singleton, A., & Toumi, R. (2013). Super-Clausius-Clapeyron scaling of rainfall in a model squall line. *Quarterly Journal of the Royal Meteorological Society*, *139*(671), 334–339. https://doi.org/10.1002/qj.1919Spinoni, J., Barbosa, P., De Jager, A., McCormick, N., Naumann, G., Vogt, J. V., et al. (2019). A new global database of meteorological drought events from 1951 to 2016. *Journal of Hydrology: Regional Studies*, *22*, 100593. https://doi.org/10.1016/j.ejrh.2019.100593Tarek, M., Brissette, F., & Arsenault, R. (2021). Uncertainty of gridded precipitation and temperature reference datasets in climate change impact studies. *Hydrology and Earth System Sciences*, *25*(6), 3331–3350. https://doi.org/10.5194/hess-25-3331-2021Tett, S. F. B., Stott, P. A., Allen, M. R., Ingram, W. J., & Mitchell, J. F. B. (1999). Causes of twentieth-century temperature change near the Earth's surface. *Nature*, *399*(6736), 569–572. https://doi.org/10.1038/21164Themeßl, M. J., Gobiet, A., & Heinrich, G. (2012). Empirical-statistical downscaling and error correction of regional climate models and its impact on the climate change signal. *Climatic Change*, *112*(2), 449–468. https://doi.org/10.1007/s10584-011-0224-4Tomas-Burguera, M., Vicente-Serrano, S. M., Peña-Angulo, D., Domínguez-Castro, F., Noguera, I., & El Kenawy, A. (2020). Global Characterization of the Varying Responses of the Standardized Precipitation Evapotranspiration Index to Atmospheric Evaporative Demand. *Journal of Geophysical Research: Atmospheres*, *125*(17), 1–14. https://doi.org/10.1029/2020JD033017Trenberth, K. E., Dai, A., Van

Der Schrier, G., Jones, P. D., Barichivich, J., Briffa, K. R., & Sheffield, J. (2014). Global warming and changes in drought. *Nature Climate Change*, *4*(1), 17–22. https://doi.org/10.1038/nclimate2067Vicente-Serrano, S. M., Beguería, S., & López-Moreno, J. I. (2010). A Multiscalar Drought Index Sensitive to Global Warming: The Standardized Precipitation Evapotranspiration Index. *Journal of Climate*, *23*(7), 1696–1718. https://doi.org/10.1175/2009JCLI2909.1Vogel, M. M., Hauser, M., & Seneviratne, S. I. (2020). Projected changes in hot, dry and wet extreme events' clusters in CMIP6 multi-model ensemble. *Environmental Research Letters*, *15*(9), 94021. https://doi.org/10.1088/1748-9326/ab90a7Wang, S., Zhang, L., She, D., Wang, G., & Zhang, Q. (2021). Future projections of flooding characteristics in the Lancang-Mekong River Basin under climate change. *Journal of Hydrology*, *602*(August), 126778. https://doi.org/10.1016/j.jhydrol.2021.126778Wells, N., Goddard, S., & Hayes, M. J. (2004). A self-calibrating Palmer Drought Severity Index. *Journal of Climate*, *17*(12), 2335–2351. https://doi.org/10.1175/1520-0442(2004)017<2335:ASPDSI>2.0.CO;2Wu, G., Chen, J., Shi, X., Kim, J., Xia, J., & Zhang, L. (2022). Impacts of global climate warming on meteorological and hydrological droughts and their propagations. *Earth's Future*. https://doi.org/10.1029/2021ef002542Wu, P., Christidis, N., & Stott, P. (2013). Anthropogenic impact on Earth's hydrological cycle. *Nature Climate Change*, *3*(9), 807–810. https://doi.org/10.1038/nclimate1932Wu, X., Hao, Z., Hao, F., Singh, V. P., & Zhang, X. (2019). Dry-hot magnitude index: a joint indicator for compound event analysis. *Environmental Research Letters*, *14*(6), 64017. https://doi.org/10.1088/1748-9326/ab1ec7Wu, X., Hao, Z., Tang, Q., Singh, V. P., Zhang, X., & Hao, F. (2020). Projected increase in compound dry and hot events over global land areas. *International Journal of Climatology*, *41*(1), 393–403. https://doi.org/10.1002/joc.6626Wu, Y., Miao, C., Sun, Y., AghaKouchak, A., Shen, C., & Fan, X. (2021). Global Observations and CMIP6 Simulations of Compound Extremes of Monthly Temperature and Precipitation. *GeoHealth*, *5*(5). https://doi.org/10.1029/2021GH000390Xu, K., Yang, D., Yang, H., Li, Z., Qin, Y., & Shen, Y. (2015). Spatio-temporal variation of drought in China during 1961–2012: A climatic perspective. *Journal of Hydrology*, *526*, 253–264. https://doi.org/10.1016/j.jhydrol.2014.09.047Xu, Z., FitzGerald, G., Guo, Y., Jalaludin, B., & Tong, S. (2016). Impact of heatwave on mortality under different heatwave definitions: A systematic review and meta-analysis. *Environment International*. https://doi.org/10.1016/j.envint.2016.02.007Yu, R., & Zhai, P. (2020). Changes in compound drought and hot extreme events in summer over populated eastern China. *Weather and Climate Extremes*, *30*, 100295. https://doi.org/10.1016/j.wace.2020.100295Zhang, P., Jeong, J. H., Yoon, J. H., Kim, H., Simon Wang, S. Y., Linderholm, H. W., et al. (2020). Abrupt shift to hotter and drier climate over inner East Asia beyond the tipping point. *Science*, *370*(6520), 1095–1099. https://doi.org/10.1126/science.abb3368Zhang, Q., Zhang, L., She, D., Wang, S., Wang, G., & Zeng, S. (2021). Automatic procedure for selecting flood events and identifying flood characteristics from daily streamflow data. *Environmental Modelling and Software*, *145*(August), 105180. https://doi.org/10.1016/j.envsoft.2021.105180Zhou, P., & Liu, Z.

(2018). Likelihood of concurrent climate extremes and variations over China. *Environmental Research Letters*, *13*(9). https://doi.org/10.1088/1748-9326/aade9eZscheischler, J., & Seneviratne, S. I. (2017). Dependence of drivers affects risks associated with compound events. *Science Advances*, *3*(6), 1–11. https://doi.org/10.1126/sciadv.1700263Zscheischler, J., Westra, S., Van Den Hurk, B. J. J. M., Seneviratne, S. I., Ward, P. J., Pitman, A., et al. (2018). Future climate risk from compound events. *Nature Climate Change*, *8*(6), 469–477. https://doi.org/10.1038/s41558-018-0156-3